Supplementary Information

Elucidating the Role of Heterojunction in Pristine Non-Fullerene Acceptor Organic Solar Cells

Anirudh Sharma[1,*], Julien Gorenflot[1], Han Xu[1], José P. Jurado[1], Shahidul Alam[1], Diego Rosas Villalva[1], Xun Pan[2], Jules Bertrandie[1], Prem Depan Nayak[1], Yakun He[1], Maryam Alqurashi[1], Ying Luo[1], Mats R. Andersson[2], Oskar J. Sandberg[3], Frederic Laquai[1], and Derya Baran[1,*]

[1]Materials Science and Engineering Program (MSE), Physical Science and Engineering Division (PSE), King Abdullah University of Science and Technology (KAUST), Thuwal 23955-6900, Kingdom of Saudi Arabia

[2]Flinders Institute for Nanoscale Science and Technology, College of Science and Engineering, Flinders University, Bedford Park 5042, Australia

[3]Physics, Faculty of Science and Engineering
Åbo Akademi University
Henrikinkatu 2, Turku 20500, Finland

*anirudh.sharma@kaust.edu.sa

*derya.baran@kaust.edu.sa

Present Address: S. A. and F. L.: Physical Chemistry and Spectroscopy of Energy Materials, Department of Chemistry, Ludwig Maximilian University of Munich, D-81377 Munich, Germany

Experimental Details:

Spectroelectrochemistry Measurements:

Materials: PEDOT:PSS (Poly(3,4-ethylenedioxythiophene) polystyrene sulfonate) (Clevios PH 1000) was obtained from Heraeus Clevios GmbH. 4 Dodecylbenzenesulfonic acid (DBSA), 3-glycidyloxypropyl trimethoxysilane (GOPS), ethylene glycol (EG), and phosphate-buffered saline (PBS) were purchased from Sigma-Aldrich. Indium tin oxide (ITO) glass substrates were sourced from Xinyan, Hong Kong.

PEDOT:PSS Dispersion Preparation: A PEDOT:PSS dispersion was prepared by mixing 5% v/v ethylene glycol, 0.002% v/v DBSA, and 1% w/w GOPS with Clevios PH 1000 under constant stirring.

Substrate Coating: ITO glass substrates were spin-coated with the PEDOT:PSS dispersion at 3000 rpm for 45 seconds. The coated substrates were then baked at 140°C for 1 hour. After baking, the substrates were immersed in deionized water for 24 hours to remove excess dopants and then dried with nitrogen gas.

Measurements:

UV-Vis Spectroscopy: UV-Vis measurements were performed using an Ocean Optics HL-2000-FHSA halogen light source. Light was transmitted via a fiber-optic cable to the polymer film in an electrochemical cell, and the transmitted light was collected using an Ocean Optics QE65 Pro Spectrometer.

Electrochemical Measurements: Cyclic voltammetry was conducted using a VSP-300 Biologic potentiostat/galvanostat. A platinum wire was used as the counter electrode, and a leakless Ag/AgCl electrode served as the reference electrode. The electrolyte used was 1× phosphate buffer saline (PBS) solution.

Procedure: The PEDOT:PSS coated ITO substrates were subjected to cyclic voltammetry in 1× PBS at a scan rate of 10 mV/s., and UV-Vis spectra were recorded simultaneously. A blank measurement was taken with uncoated ITO substrates to calibrate the Ocean View software before the PEDOT:PSS was measured.

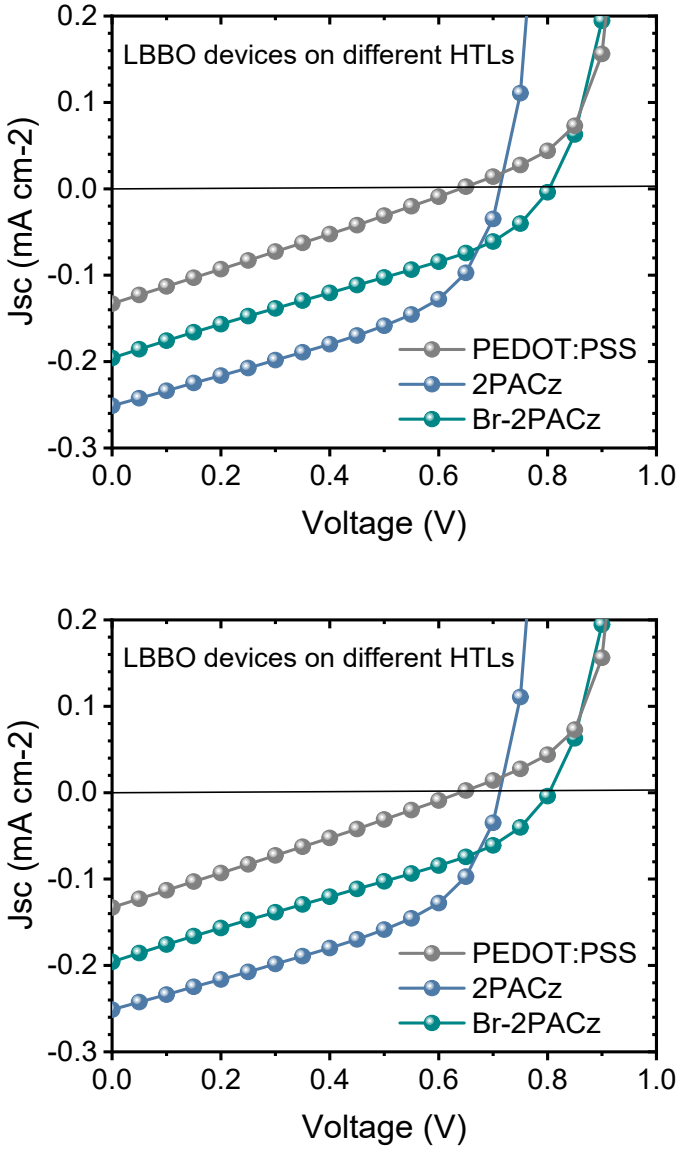

Figure S1. J-V characteristics of L8BO OSCs utilizing PEDOT:PSS and SAM-based *p*-type interlayers.

Table S1. Summary of J-V parameters of L8BO OSCs utilizing PEDOT:PSS and SAM-based HTLs. The active area of the devices was 0.1 cm^{-2}. J-V parameters of over 20 devices with L8BO as the PAL and CuSCN as the HTL are also summarized to demonstrate the statistical reproducibility of photovoltaic parameters.

PAL	Interlayer	Jsc (mA cm^{-2})	Voc(V)	FF (%)	PCE (%)
L8BO					

	2PACz	0.25	0.71	45	0.08
	Br2PACz	0.19	0.80	32	0.05
L8BO with PM6					
0 wt.% PM6	PEDOT:PSS	0.09	0.746	27	0.02
2 wt.% PM6		4.08	0.899	40	1.48
5 wt.% PM6		14.20	0.907	60	7.77
9 wt.% PM6		19.10	0.898	69	11.88
L8BO					
	CuSCN	7.24	0.864	56	3.52
		7.29	0.864	56	3.56
		7.52	0.866	58	3.80
		7.17	0.859	57	3.51
		7.49	0.863	58	3.77
		7.42	0.868	59	3.83
		7.26	0.858	60	3.71
		7.09	0.855	60	3.62
		7.59	0.882	57	3.83
		7.36	0.880	58	3.77
		7.43	0.872	59	3.81
		7.33	0.884	56	3.66
		7.86	0.866	61	4.20
		7.63	0.871	61	4.07
		7.40	0.878	59	3.82
		7.67	0.868	61	4.08
		7.61	0.867	61	4.02
		7.62	0.865	60	3.99

7.23	0.883	57	3.66
7.53	0.869	62	4.08
7.36	0.878	59	3.82
7.34	0.868	62	3.93
7.14	0.877	57	3.58

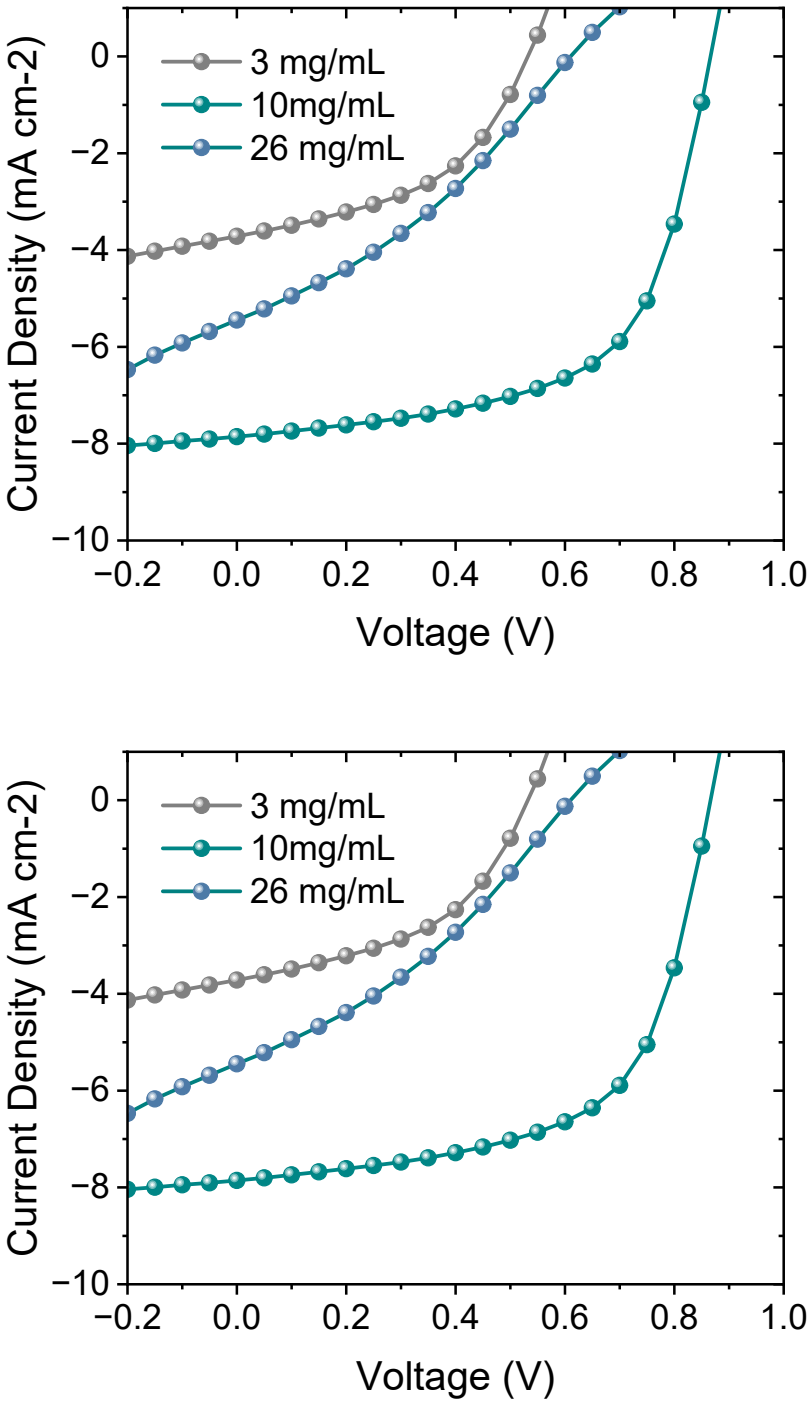

Figure S2: J-V curves of L8BO devices with CuSCN HTL deposited via different concentrations of CuSCN solution.

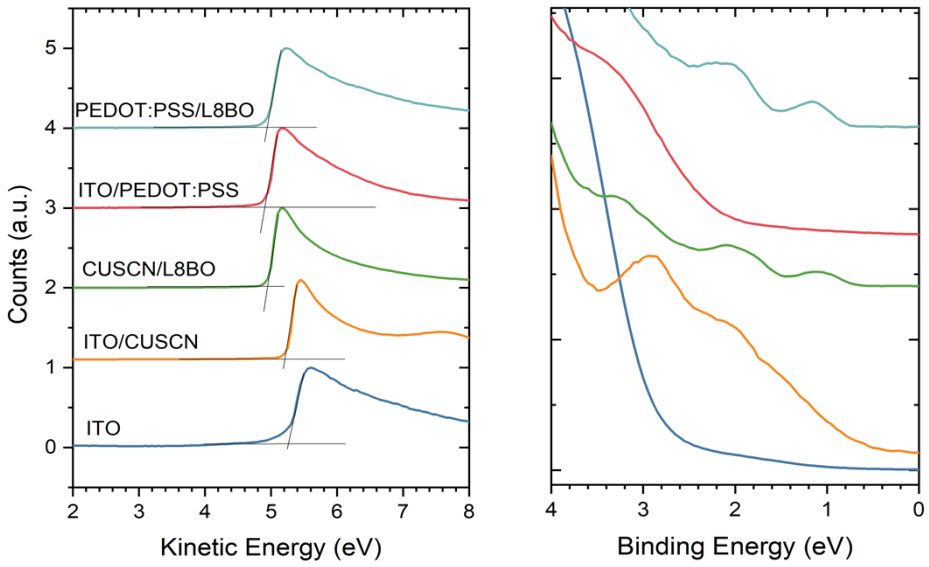

Figure S3: UPS spectra of CuSCN and PEDOT:PSS deposited on ITO, and L8BO deposited on CuSCN/ITO and PEDOT:PSS/ITO.

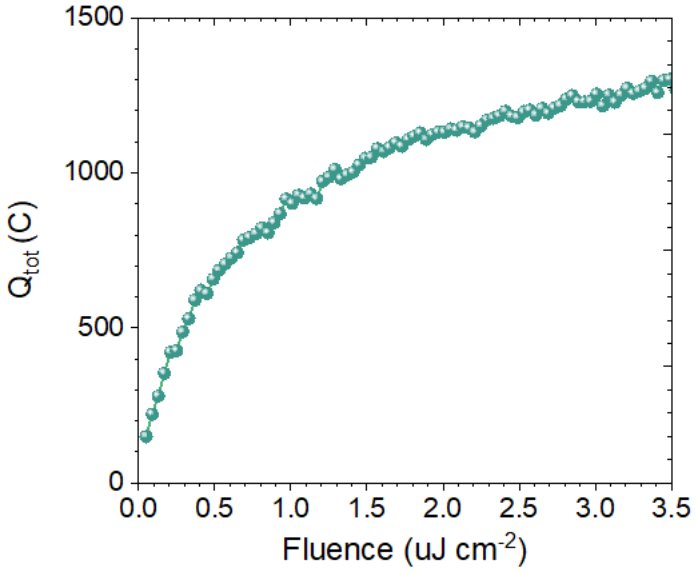

Figure S4: Total extracted charge (Q_{tot}) as a function of laser fluence in TDCF measurement.

Table S2. Summary of photovoltaic parameters of best performing L8BO devices with varying amounts of donor polymer PM6 and PIDT-T8BT fabricated using CuSCN as the hole transport layer. The average PCE shown in parenthesis was determined over six devices.

Donor content [%]	Jsc [mAcm^{-2}]	Jsc Integrated [mAcm^{-2}]	Voc [mV]	FF [%]	PCE [%]
PM6:L8BO					
0	7.9	6.8	0.866	61	4.2 (4.0 ± 0.2)
2	10.6	10.5	0.864	57	5.2 (5.1 ± 0.2)
5	15.2	13.2	0.863	60	7.9 (7.7 ± 0.2)
9	19.6	17.6	0.853	63	10.5 (10.3 ± 0.2)
17	21.8	19.3	0.853	69	12.7 (12.6 ± 0.2)
45	23.3	22.5	0.843	71	14 (13.7 ± 0.3)
PIDT-T8BT:L8BO					
2	10.4	10.2	0.840	54	4.7 (4.4 ± 0.4)
5	14.6	13.0	0.845	53	6.5 (6.3 ± 0.2)
9	15.8	14.1	0.862	55	7.5 (7.3 ± 0.3)
17	15.7	14.0	0.853	50	6.7 (6.6 ± 0.1)

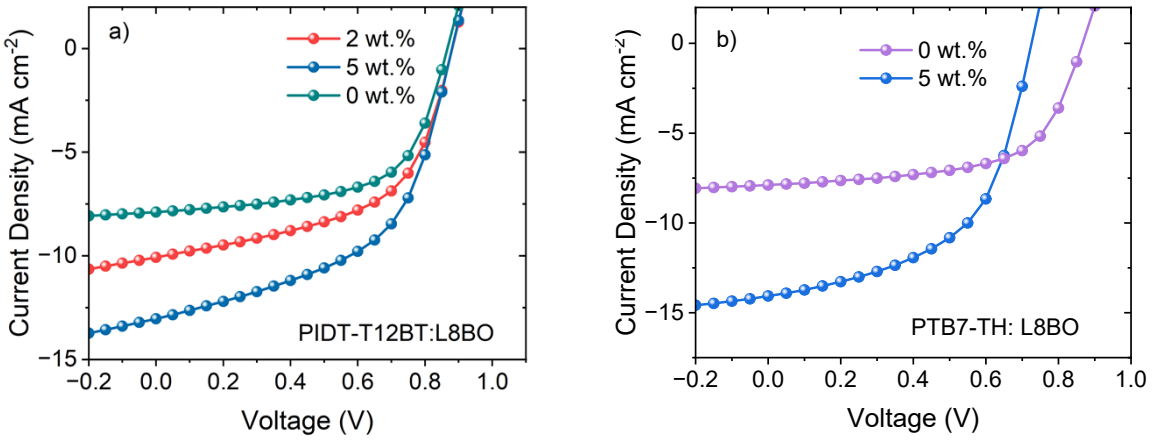

Figure S5: J-V curves of L8BO devices with varying amounts of donor polymers.

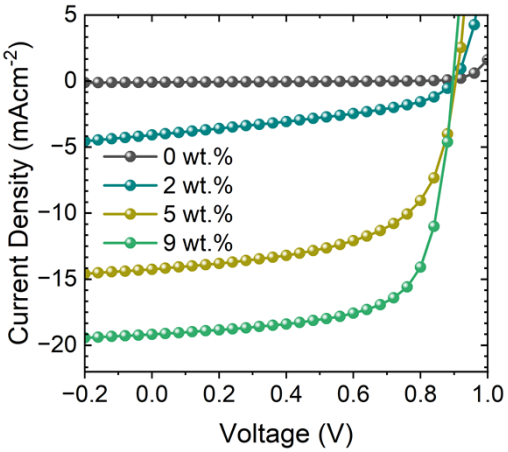

Figure S6: J-V curves of L8BO devices without and with varying amounts of PM6, and using PEDOT:PSS HTL.

Table S3: Summary of energy levels: work function (Φ), ionization energy (IE), electron affinity (EA) measured for L8BO, and its respective BHJ blends with 10 wt.% polymers-PM6, PIDT-T8BT, and PTB7-TH deposited on CuSCN, and PM6-L8BO BHJ deposited on PEDOT:PSS coated ITO. The reproducibility of UPS and LE-IPES derived values including the experimental uncertainty is ± 0.1 eV.

Material	Φ (eV)	HOMO onset (donor) (eV)	HOMO onset (acceptor) (eV)	IE_{donor} (eV)	$IE_{acceptor}$ (eV)	EA (eV)
HTL: L8BO and polymer-L8BO BHJ deposited on CuSCN/ITO						
L8BO	4.95	-	0.69	-	5.65	3.95
PM6-L8BO	4.92	0.36	0.73	5.28	5.65	3.78
PIDT:T8BT-L8BO	4.82	0.41	0.77	5.23	5.59	3.95
PTB7-Th-L8BO	4.79	0.20	0.57	4.99	5.36	3.85
HTL: L8BO and PM6-L8BO BHJ deposited on PEDOT:PSS/ITO						
L8BO	4.92	-	0.83	-	5.75	3.93
PM6-L8BO	5.04	0.33	0.78	5.37	5.82	3.85
ETL: PNDIT-F3N deposited on PM6-L8BO/PEDOT:PSS/ITO						

Material	Φ (eV)	HOMO onset (eV)	IE (eV)	EA (eV)
PNDIT-F3N/PM6-L8BO	3.81	1.91	5.72	3.50

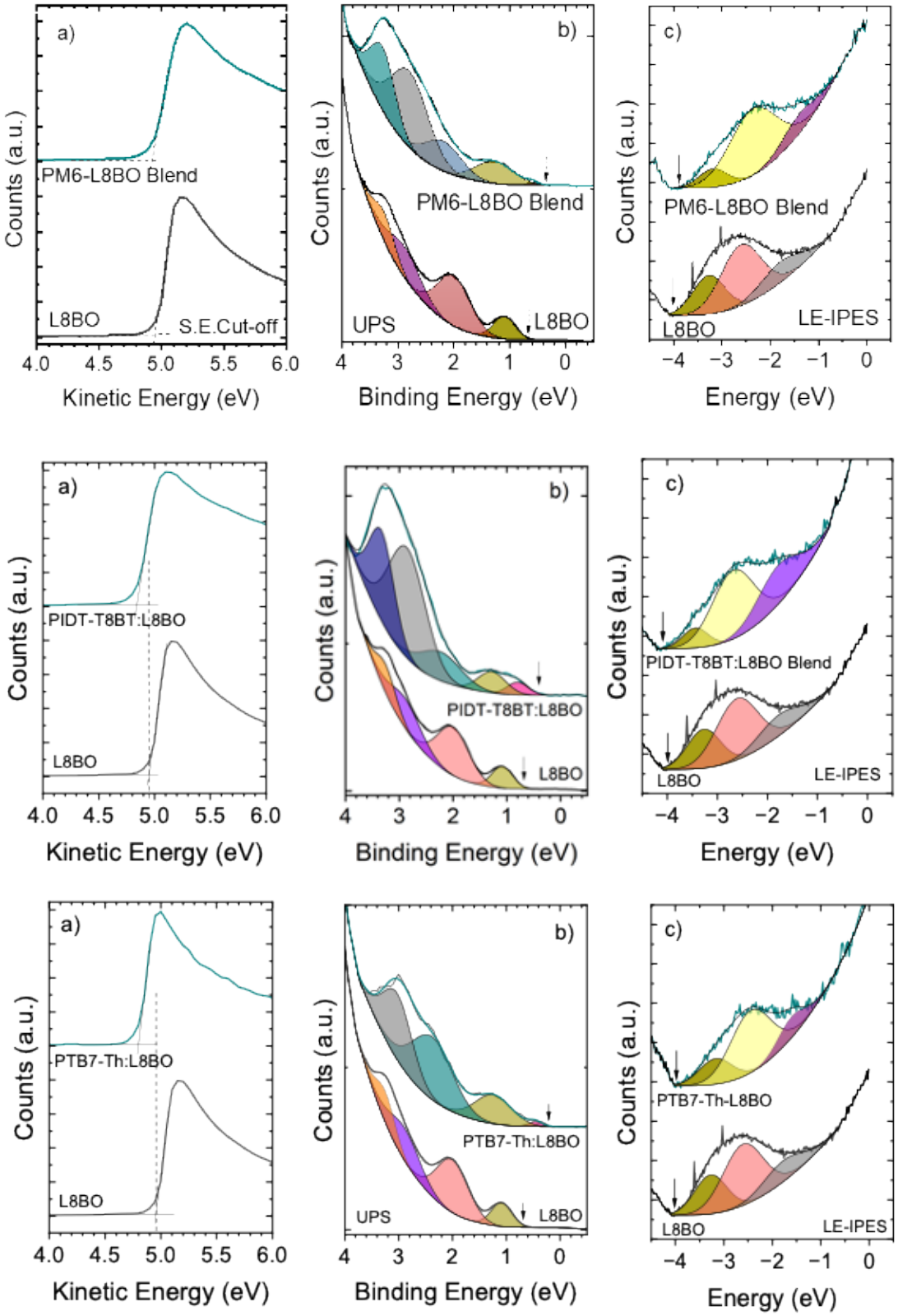

Figure S7: UPS (a, b) and LE-IPES (c) spectra of PM6 (10 wt.%): L8BO, PIDT-T8BT (10 wt.%):L8BO, and PTB7-Th (10 wt.%): L8BO BHJ blend deposited on CuSCN coated ITO mimicking a device stack.

For probing the energetics of D/A BHJ blends, a donor amount of 10 wt.% in solution results in a D/A ratio of close to 1:1 on the thin film surface, which makes it more representative of the D/A ratio in a real device. The amounts of donor polymer higher than 10 wt. % in solutions often results in surface saturation of donor polymer on the film surface. This limits the determination of energetics of both donor and acceptor phases in blends via UPS and LE-IPES, since the polymer saturation on the film surface results in spectral properties identical to that of neat polymer since the probing depth of UPS is approximately 2-3 nm.

Grazing Incidence Wide Angle X-ray Scattering (GIWAXS)

Films were spin-coated on polished silicon substrates from $CHCL_3$ solution with 0.5% DIO. Data was acquired using a Xenocs Xeuss 3.0 equipped with a Genix 3D Cu source with a parallel collimation $\lambda = 1.54$ Å.

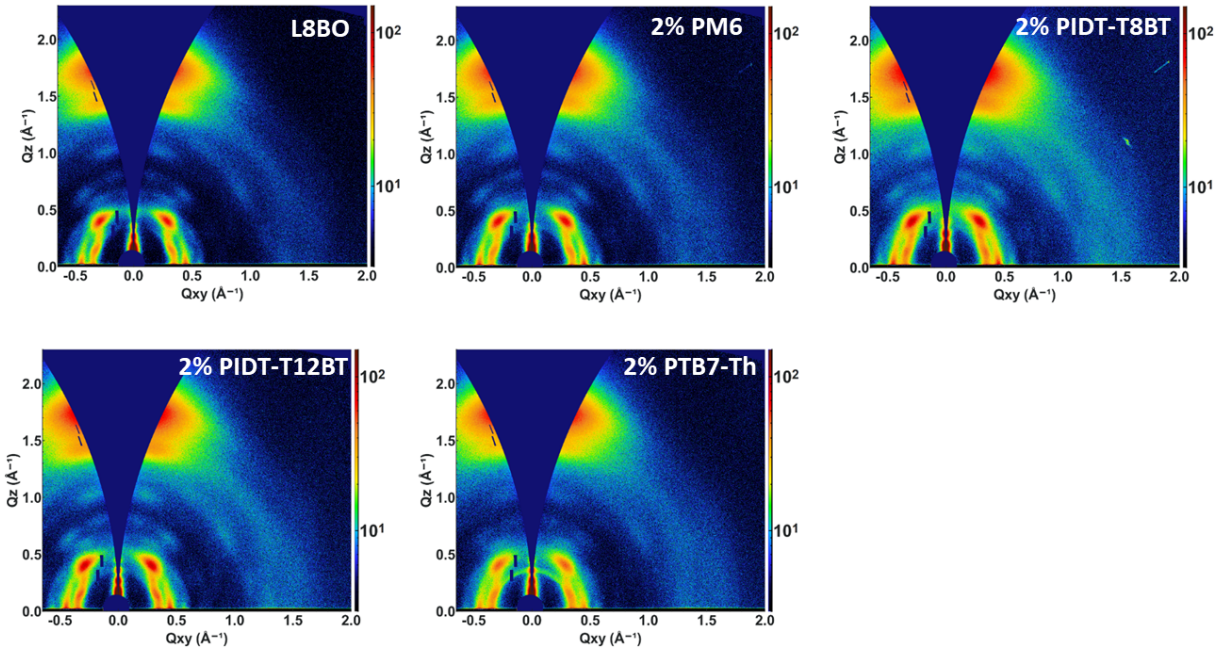

Figure S8: GIWAXS of L8BO and L8BO blends with 2 wt.% of different donor polymers cast from $CHCl_3$ (with 0.5% DIO).

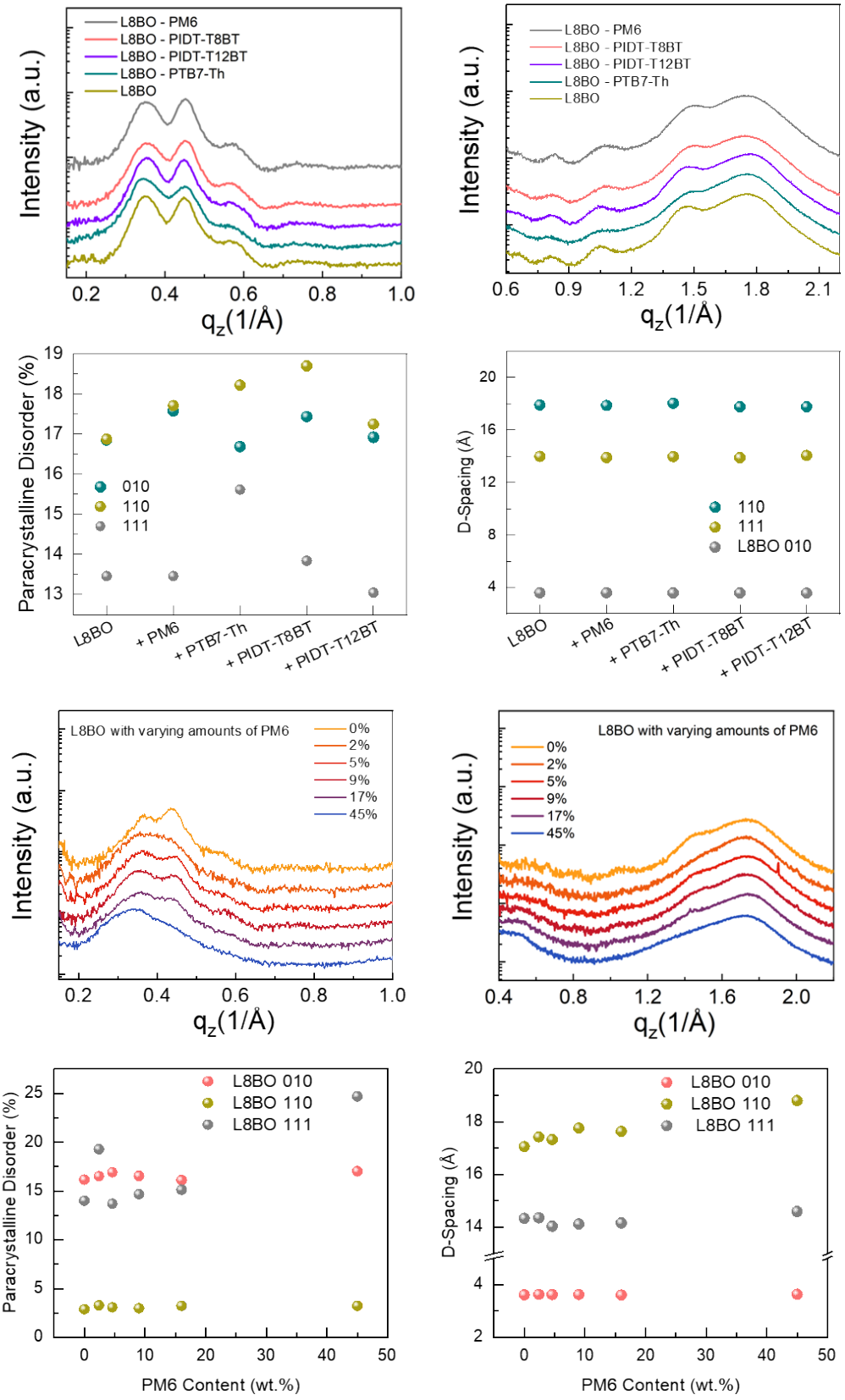

Figure S9: GIWAXS line-cuts and the calculated para-crystalline disorder and D-spacing of L8BO and L8BO blends with 2 wt.% of different donor polymers cast from CHCl3 (with 0.5% DIO), as well as with increasing amount of PM6 from 2 wt.% to 45 wt.%.

Transient Absorption Spectroscopy (TAS)

Spectral signature of the L8BO's excited species:

(i) Initially (300 - 450 fs after excitation), all films exhibit the same spectral signature upon L8BO selective excitation at 730 to 750 nm (Figure S10 and S11a-c), thus assigned to **L8BO singlet excitons**. Its main features are a broad ground state bleach (GSB) band from 1.45 to 2.1 eV and photoinduced absorption (PA) between 1.23 and 1.45 eV, peaking around 1.37 - 1.39 eV. On neat L8BO films on quartz, a clear electroabsorption feature was additionally present, peaking negatively at 1.39 and positively at 1.46 eV but decayed faster than the rest of the exciton signal (*vide infra*).

(ii) **Charge spectra** dominate the longer delay spectra of optimal PM6:L8BO blends (Figure S10 and S11g, j). A key feature is the PA band at 1.1 to 1.4 eV, peaking around 1.25 eV, particularly the part between 1.1 and 1.22 eV that does not overlap with the PA of other species. Importantly this band is partly caused by the charges in L8BO (not only PM6) as seen in CuSCN/L8BO and PEDOT/L8BO films and can be used to probe charges.

(iii) Finally, nanosecond spectra of neat L8BO films on quartz exhibit a weak positive signal from 1 to 1.4 eV on the hundreds of ps to ns timescale, which we tentatively assign to the rise of a **triplet states** population, superposing the signal from the long live tail of the density of the singlet excitons. This feature becomes prominent in the presence of PEDOT:PSS, as detailed below, but is also present in L8BO on glass and CuSCN. It also strongly differs from PEDOT charges as can be obtained by spectroelectrochemistry on films[1] (also see Figure S10e-f). The nature of this feature is not totally clear, while its maximum is observed close to 1.45 eV in pristine material (Figure S12), which is compatible with ground state photo bleach, its extension as low as 1 eV is highly surprising. Possible hypothesis is photobleach of subbandgap absorption, stimulated emission via a thermally assisted delayed fluorescence type mechanism, or that the triplets would have a CT-character, generating some electroabsorption. A hint towards its attribution to triplet states is that it is clearly associated with a PA peak maximizing around 0.85 eV, which is identified as a triplet signature in spectra using a triplet sensitizer (see Figure S18).

(iv) Notably, the negative peak observed around 0.8 eV is associated with both singlet and triplet species. The presence of singlet excitons is supported by their detection in the neat L8BO film on quartz at short delay times (from picoseconds to nanoseconds). Triplet excitons, on the other hand, are indicated by the enhancement of this peak upon addition of

the triplet sensitizer PtOEP, as shown in Figure S18. The previously mentioned positive signal between 1 and 1.4 eV (see note iii) also appears alongside the negative triplet signal. However, this positive feature is absent in the PtOEP-sensitized sample, potentially due to being overshadowed by a stronger negative signal.

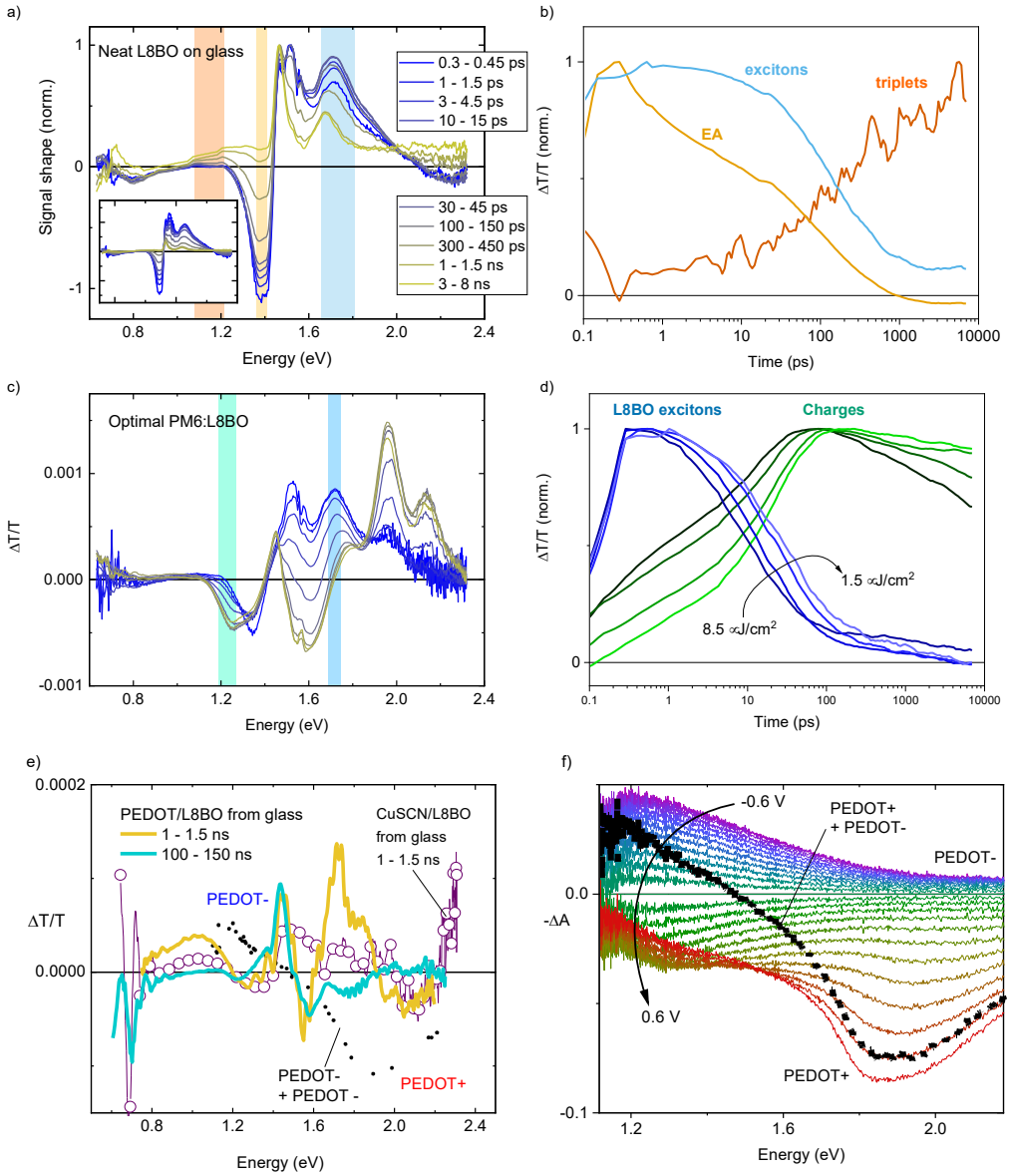

Figure S10: Reference TA spectra for excited species. (a) Spectral shape of the excited state signal from neat L8BO on glass upon film side excitation of 1.3 μJ/cm^2 at 750 nm at different delays following the excitation. The evolution of the spectral shape shows the formation of a different long live species. The shaded areas are those whose kinetics are represented in panel (b). The non-normalized spectra are shown in the inset. The labels next to the curves indicate the dominating (but not unique) contribution in that spectral region. EA stands for electroabsorption. (c) Spectra of the excited states formed on an optimal PM6:L8BO film upon film side excitation of 1.5 μJ/cm^2 at 750 nm. The delays represented are the same as on panel (a). Note that the signal strength i.e. the density of excited species remains almost unchanged

with increasing the delay, indicating the efficient formation of long lived species. The shaded area represent spectral regions with no contribution from excitons (around 1.2 eV) and charges (around 1.67 eV), whose kinetics thus represent the charges, and exciton dynamics, respectively (shown in panel (d) with their fluence dependence). Panel (e) shows the comparison of the long live species obtained on PEDOT/L8BO films (excited at 730 nm, 1.1 μJ/cm^2) with PEDOT charges as obtained from spectroelectrochemistry on PEDOT:PBS films (panel (f)). Note that although the reference material used here was PEDOT:PbS instead of PEDOT:PSS, the PEDOT:PSS has been previously shown to exhibit the same charge spectra.[1]

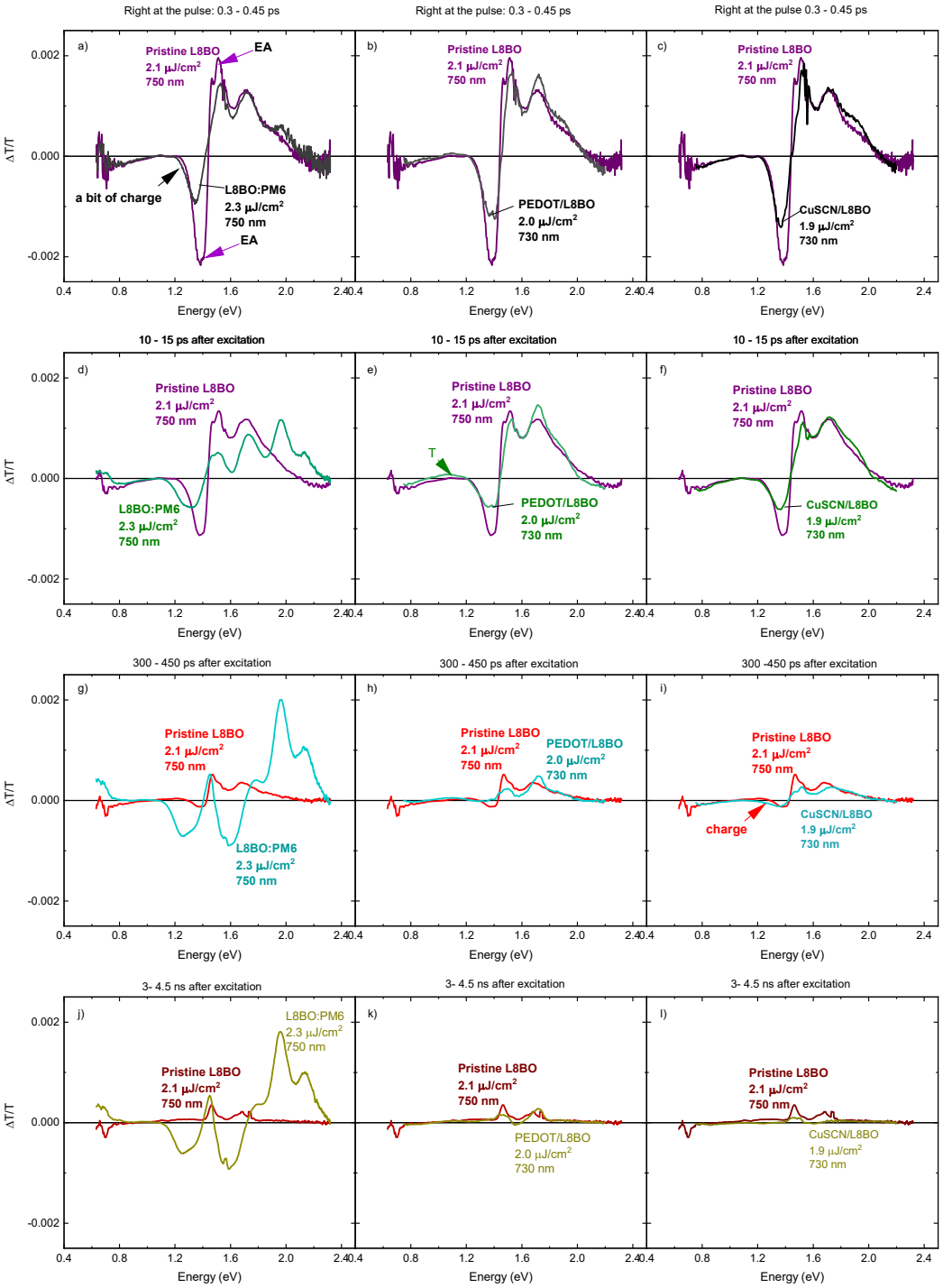
Right at the pulse: 0.3 - 0.45 ps
Right at the pulse: 0.3 - 0.45 ps
Right at the pulse 0.3 - 0.45 ps
a)
Pristine L8BO
2.1 μJ/cm²
750 nm
EA
a bit of charge
L8BO:PM6
2.3 μJ/cm²
750 nm
EA
b)
Pristine L8BO
2.1 μJ/cm²
750 nm
PEDOT/L8BO
2.0 μJ/cm²
730 nm
c)
Pristine L8BO
2.1 μJ/cm²
750 nm
CuSCN/L8BO
1.9 μJ/cm²
730 nm
ΔT/T
Energy (eV)
10 - 15 ps after excitation
10 - 15 ps after excitation
10 - 15 ps after excitation
d)
Pristine L8BO
2.1 μJ/cm²
750 nm
L8BO:PM6
2.3 μJ/cm²
750 nm
e)
Pristine L8BO
2.1 μJ/cm²
750 nm
T
PEDOT/L8BO
2.0 μJ/cm²
730 nm
f)
Pristine L8BO
2.1 μJ/cm²
750 nm
CuSCN/L8BO
1.9 μJ/cm²
730 nm
300 - 450 ps after excitation
300 - 450 ps after excitation
300 -450 ps after excitation
g)
Pristine L8BO
2.1 μJ/cm²
750 nm
L8BO:PM6
2.3 μJ/cm²
750 nm
h)
Pristine L8BO
2.1 μJ/cm²
750 nm
PEDOT/L8BO
2.0 μJ/cm²
730 nm
i)
Pristine L8BO
2.1 μJ/cm²
750 nm
charge
CuSCN/L8BO
1.9 μJ/cm²
730 nm
3- 4.5 ns after excitation
3- 4.5 ns after excitation
3- 4.5 ns after excitation
j)
L8BO:PM6
2.3 μJ/cm²
750 nm
Pristine L8BO
2.1 μJ/cm²
750 nm
k)
Pristine L8BO
2.1 μJ/cm²
750 nm
PEDOT/L8BO
2.0 μJ/cm²
730 nm
l)
Pristine L8BO
2.1 μJ/cm²
750 nm
CuSCN/L8BO
1.9 μJ/cm²
730 nm

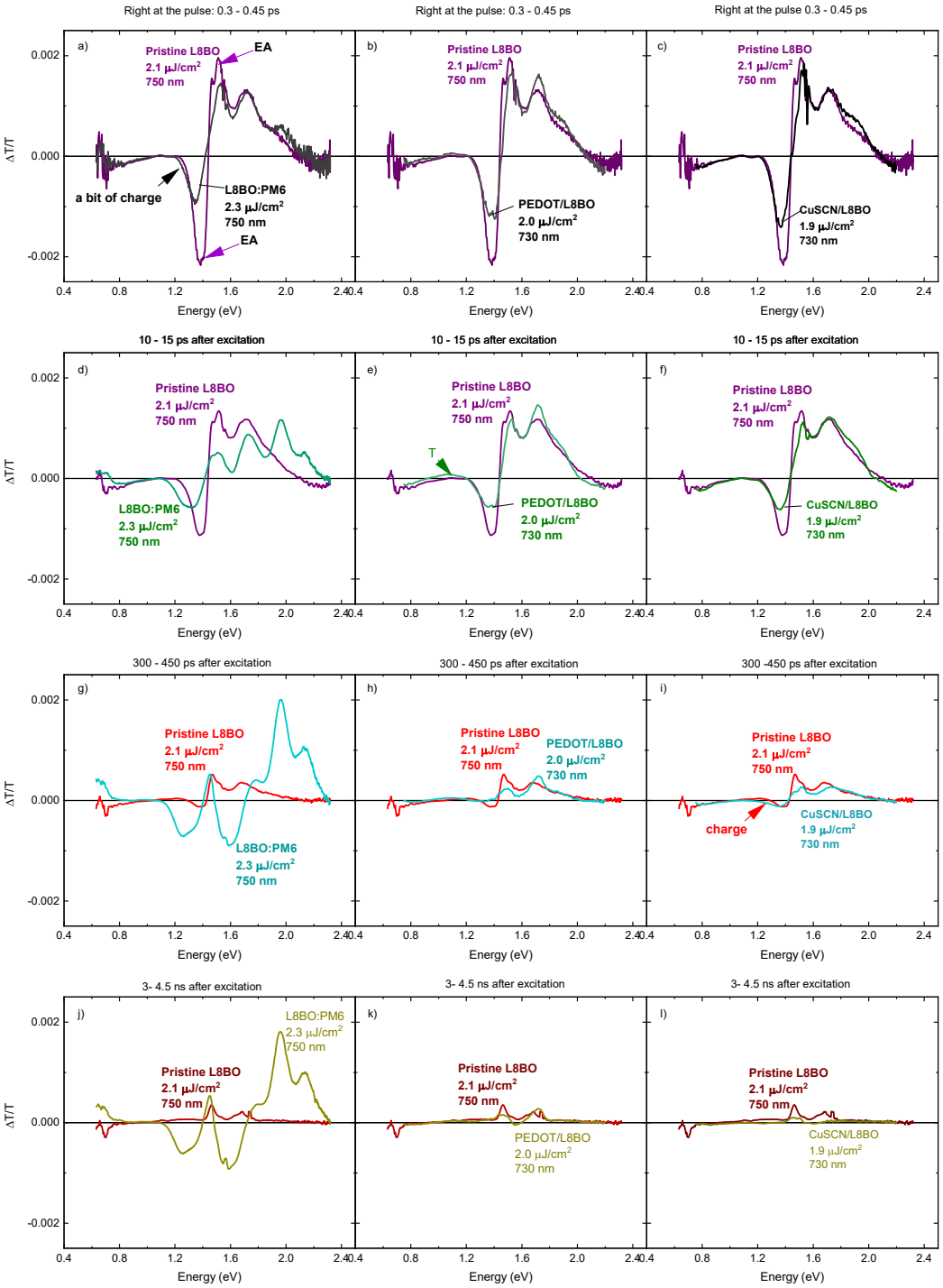

Figure S11: **Compared TA signal evolution ps-ns range, low-intensity excitation.** The samples with HTL were excited from the HTL (glass) side, the reference samples from the film side.

Charge transfer character of the primary photoexcitation in quartz/L8BO films:

A somewhat confusing aspect, is that while not exhibiting charge signature, quartz/L8BO spectra exhibit shortly after excitation a feature strongly resembling electroabsorption (EA), which suggests that the primary photogenerated species does possess a strong charge transfer (CT) character.[2] However, this feature decays without evolving into actual charge signature, and actually faster than the rest of the exciton signal, on a fluence-independent fashion, and without overall loss of excitation density (indicated by the stable photobleach, see figure S12). This suggests a relaxation where initially generated exciton lose their CT-character, possibly upon relaxation to more localized (intramolecular) states. Importantly, we did not observe such a strong EA in any of the systems for which we have evidence of photocurrent generation (see PM6:L8BO, L8BO on CuSCN, and L8BO on PEDOT:PSS in Figure S11 a-c), indicating the associated L8BO CT-excitons are not involved in the reported photocurrent generation.

Intensity of the charge signal in HTL/L8BO

In contrast to the bulk of L8BO, the HTL/L8BO interface does appear to generate charges. We note that the charge signal observed in the nanosecond time scale on HTL/L8BO films remained modest, similar in intensity to the singlets and triplets remaining in the nanosecond time range in the absence of HTL (see Figures S13a-b). Similarly, the charge formation did not significantly reduce the exciton lifetime (Figure S14). This lifetime is indeed probably more strongly limited by exciton-exciton annihilation due to the rather large fluences required by TA experiments. We note that the situation would likely be more favorable under one sun condition, as the absence of exciton-exciton annihilation would give excitons more time to reach the HTL/PAL interface.

CuSCN and PEDOT:PSS do not seem to have different effects on charge generation efficiency on samples excited from the interface side. However, when exciting from the L8BO side, more charges are generated by the CuSCN/L8BO interface than by the PEDOT:PSS/L8BO (Figure S17), suggesting a better diffusion of the excitons to that interface, which could be due to a larger interpenetration of the HTL and the PAL, or to a molecular stacking more favorable to exciton diffusion when L8BO is deposited on CuSCN. Moreover, in PEDOT:PSS, charge generation is accompanied at all fluences by a triplet generation, possibly due to early charge recombination. In contrast, with CuSCN, triplet formation becomes important and only visible at higher fluences (see Figure S13d).

This interface quenching effect is also seen when comparing the fate of charges generated in the bulk, compared to those generated at the interface. Adding 2 wt.% of PM6 to the L8BO enables generation in the bulk of the active layer (see Figure S15). By exciting specifically in the bulk (excitation from the PAL side at a wavelength having a low penetration depth) CuSCN/PM6 (2 wt.%):L8BO and PEDOT:PSS/PM6 (2 wt.%):L8BO exhibit the same charge lifetime (Figure S17a). On the opposite, interface excitation results in a much faster decay if the HTL is PEDOT:PSS (Figure S17a).

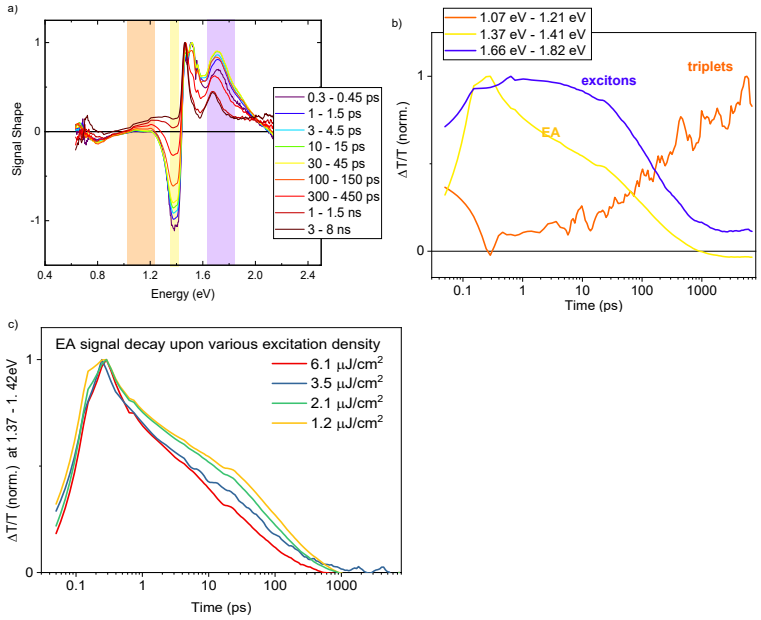

Figure S12: Electroabsorption is present on L8BO films on quartz (a) but decays faster than other species (b), and this decay is mostly fluence independent (c). Note: the remaining fluence dependence is most likely due to the exciton and triplets contribution PA in that region. Panels (a-b) correspond to the 1.2 μJ/cm² fluence. The film was excited at 750 nm.

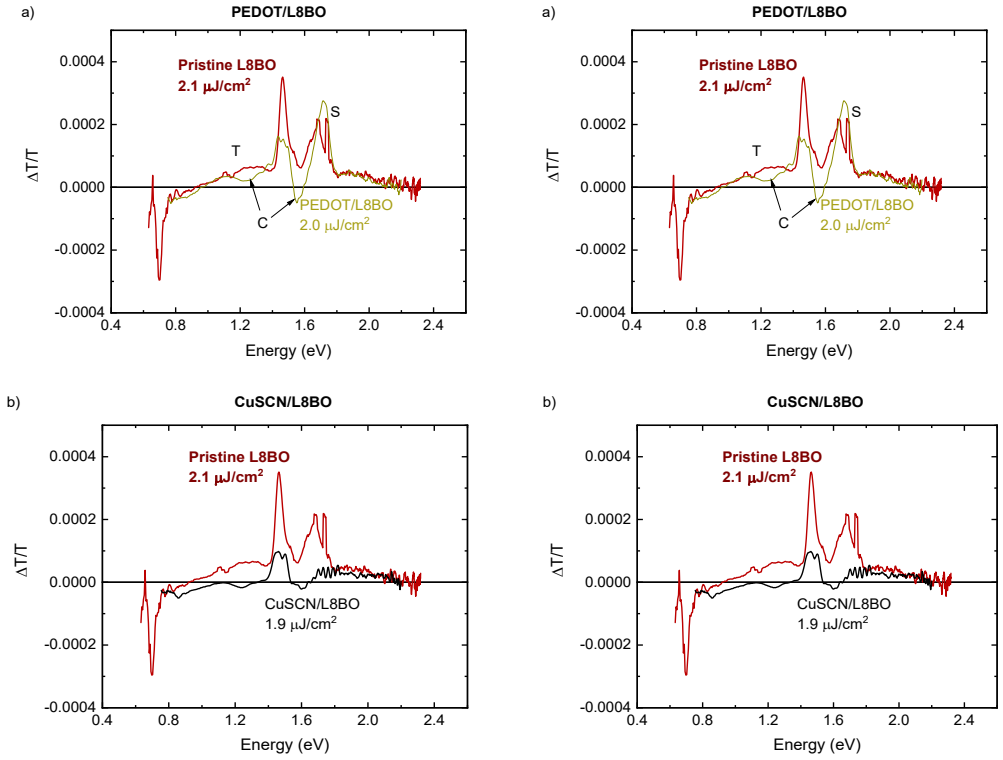

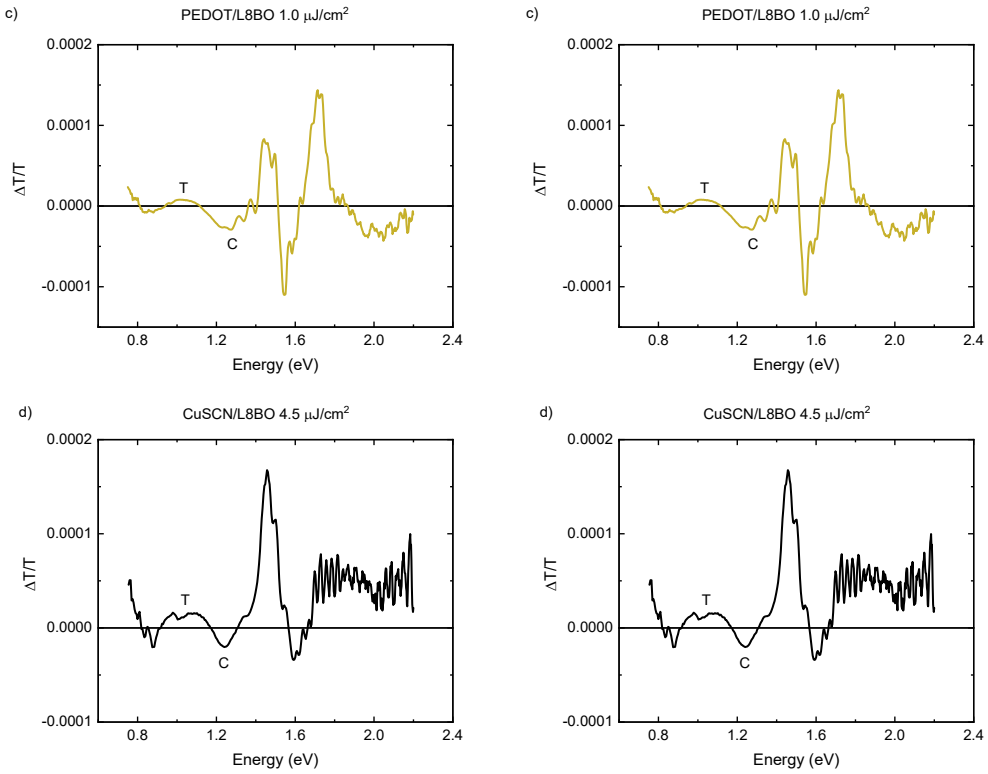

Figure S13: Spectra signature of long-lived species (3 - 4.5 ns) obtained on L8BO films depending on the layer below (quartz, CuSCN, PEDOT:PSS), as well as the fluence dependence of these signatures. While for similar fluences (a,b) films on PEDOT:PSS appear to form more triplets than those on CuSCN, increasing the fluence, also leads to important triplet formation in CuSCN (d). Reciprocally. Decreasing the fluence on PEDOT:PSS/L8BO films decreases the triplet contribution (c). The films were excited at 730 nm from the HTL (glass) side (and from the film side for the quartz/L8BO reference).

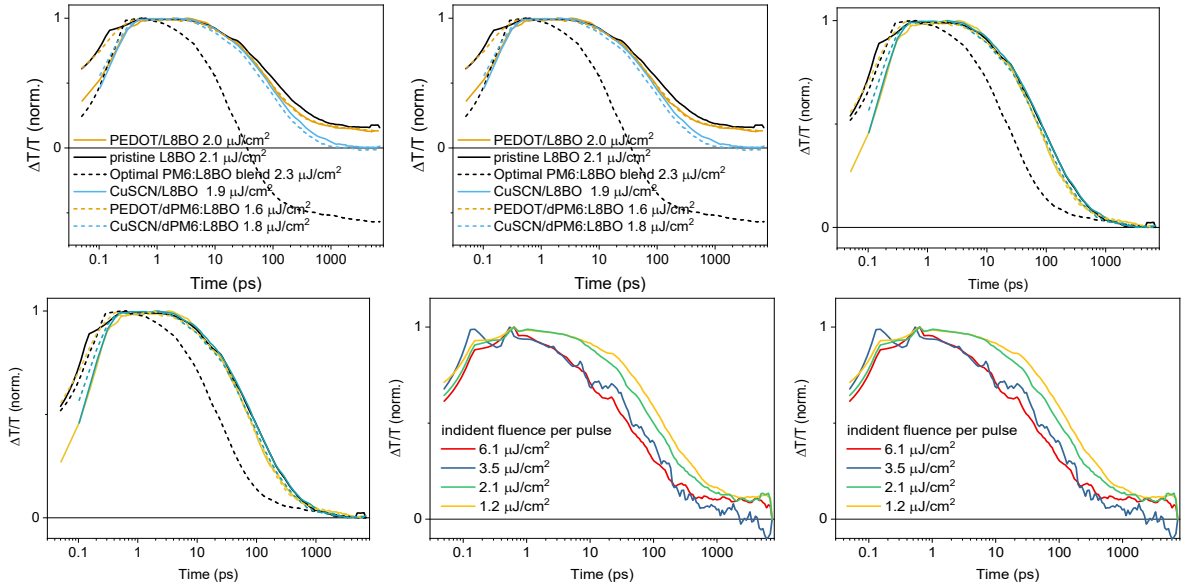

Figure S14: Left: signal dynamics 1.64 – 1.69 eV (mostly singlet excitons) of the different films using HTL-side illumination at 730 nm except for the references without HTL: film side illumination at 750 nm. Middle: normalized from 0-1 to remove the contribution of the long lived signal species. Right: fluence dependence of the exciton dynamics (L8BO on quartz

excited at 750 nm from the film side) showing that the exciton lifetime is limited by singlet-singlet annihilation in the probed range of excitation fluences.

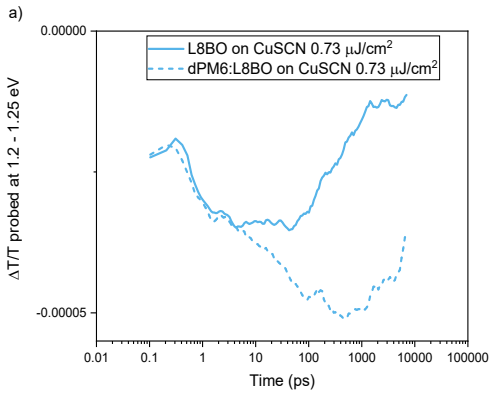
a)
L8BO on CuSCN 0.73 μJ/cm²
dPM6:L8BO on CuSCN 0.73 μJ/cm²
ΔT/T probed at 1.2 - 1.25 eV
0.00000
-0.00005
0.01
0.1
1
10
100
1000
10000
100000
Time (ps)

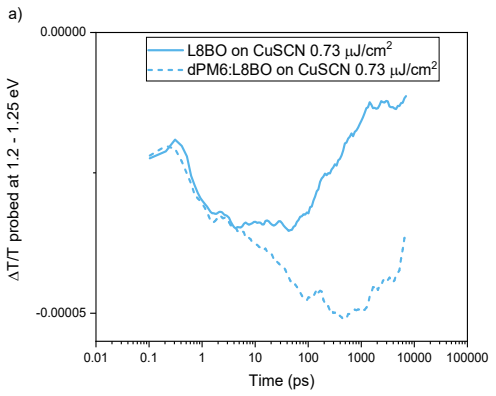
a)
L8BO on CuSCN 0.73 μJ/cm²
dPM6:L8BO on CuSCN 0.73 μJ/cm²
ΔT/T probed at 1.2 - 1.25 eV
0.00000
-0.00005
0.01
0.1
1
10
100
1000
10000
100000
Time (ps)

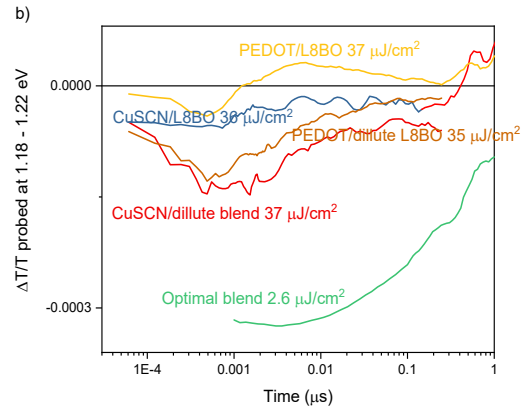
b)
PEDOT/L8BO 37 μJ/cm²
CuSCN/L8BO 36 μJ/cm²
PEDOT/dillute L8BO 35 μJ/cm²
CuSCN/dillute blend 37 μJ/cm²
Optimal blend 2.6 μJ/cm²
ΔT/T probed at 1.18 - 1.22 eV
0.0000
-0.0003
1E-4
0.001
0.01
0.1
1
Time (μs)

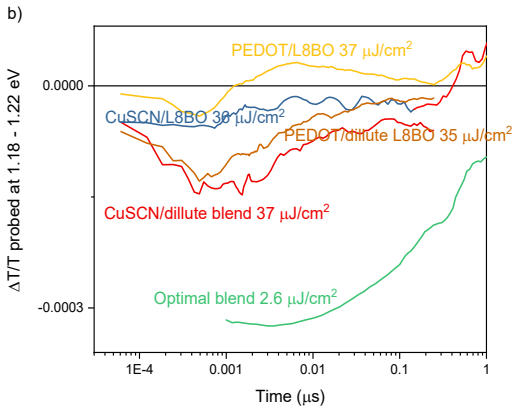
b)
PEDOT/L8BO 37 μJ/cm²
CuSCN/L8BO 36 μJ/cm²
PEDOT/dillute L8BO 35 μJ/cm²
CuSCN/dillute blend 37 μJ/cm²
Optimal blend 2.6 μJ/cm²
ΔT/T probed at 1.18 - 1.22 eV
0.0000
-0.0003
1E-4
0.001
0.01
0.1
1
Time (μs)

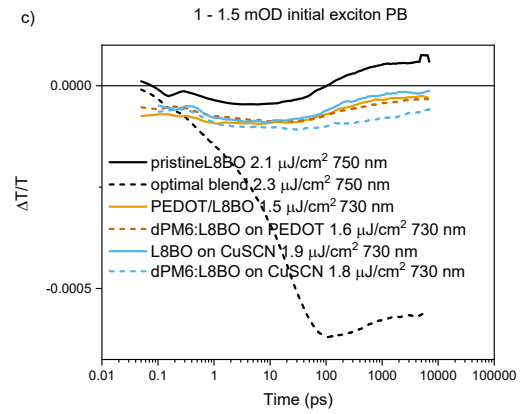
c)
1 - 1.5 mOD initial exciton PB
pristineL8BO 2.1 μJ/cm² 750 nm
optimal blend 2.3 μJ/cm² 750 nm
PEDOT/L8BO 1.5 μJ/cm² 730 nm
dPM6:L8BO on PEDOT 1.6 μJ/cm² 730 nm
L8BO on CuSCN 1.9 μJ/cm² 730 nm
dPM6:L8BO on CuSCN 1.8 μJ/cm² 730 nm
ΔT/T
0.0000
-0.0005
0.01
0.1
1
10
100
1000
10000
100000
Time (ps)

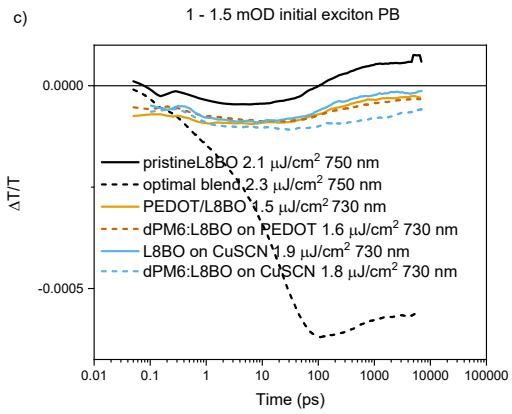
c)
1 - 1.5 mOD initial exciton PB
pristineL8BO 2.1 μJ/cm² 750 nm
optimal blend 2.3 μJ/cm² 750 nm
PEDOT/L8BO 1.5 μJ/cm² 730 nm
dPM6:L8BO on PEDOT 1.6 μJ/cm² 730 nm
L8BO on CuSCN 1.9 μJ/cm² 730 nm
dPM6:L8BO on CuSCN 1.8 μJ/cm² 730 nm
ΔT/T
0.0000
-0.0005
0.01
0.1
1
10
100
1000
10000
100000
Time (ps)

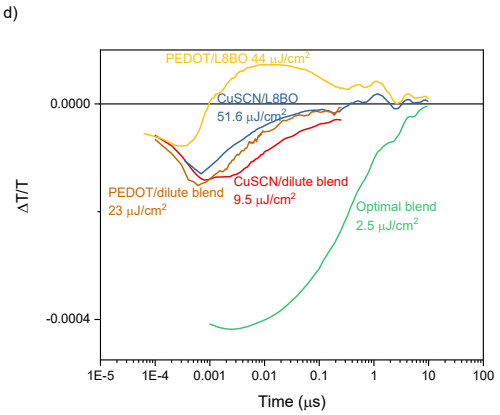
d)
PEDOT/L8BO 44 μJ/cm²
CuSCN/L8BO
51.6 μJ/cm²
PEDOT/dilute blend
23 μJ/cm²
CuSCN/dilute blend
9.5 μJ/cm²
Optimal blend
2.5 μJ/cm²
ΔT/T
0.0000
-0.0004
1E-5
1E-4
0.001
0.01
0.1
1
10
100
Time (μs)

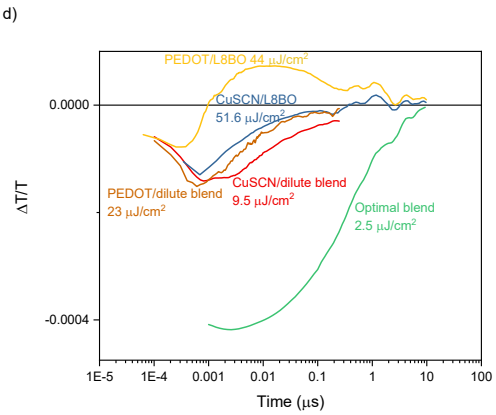
d)
PEDOT/L8BO 44 μJ/cm²
CuSCN/L8BO
51.6 μJ/cm²
PEDOT/dilute blend
23 μJ/cm²
CuSCN/dilute blend
9.5 μJ/cm²
Optimal blend
2.5 μJ/cm²
ΔT/T
0.0000
-0.0004
1E-5
1E-4
0.001
0.01
0.1
1
10
100
Time (μs)

Figure S15: Impact of 2% PM6 addition on charge generation: (a) with the addition of PM6 the charge signal increases during a longer time (panel a: charge photoinduced absorption dynamics upon low fluence excitation at 730 nm from the HTL side), overall reaching larger charge density. (b) The generation efficiency difference is larger upon 532 nm excitation as most of the light is absorbed far from the HTL:PAL interface (panel b: charge photoinduced absorption dynamics upon 532 nm excitation from the HTL side (film side for the 2 samples that have no HTL)) for similar excitation fluences, except for the optimal blend where a fluence in this range would give a too large signal. (c) Little difference in generated charge signal intensity is observed between PEDOT and CuSCN. (d) Compared decays upon similar initial charge signal (see normalized version in Figure 4).

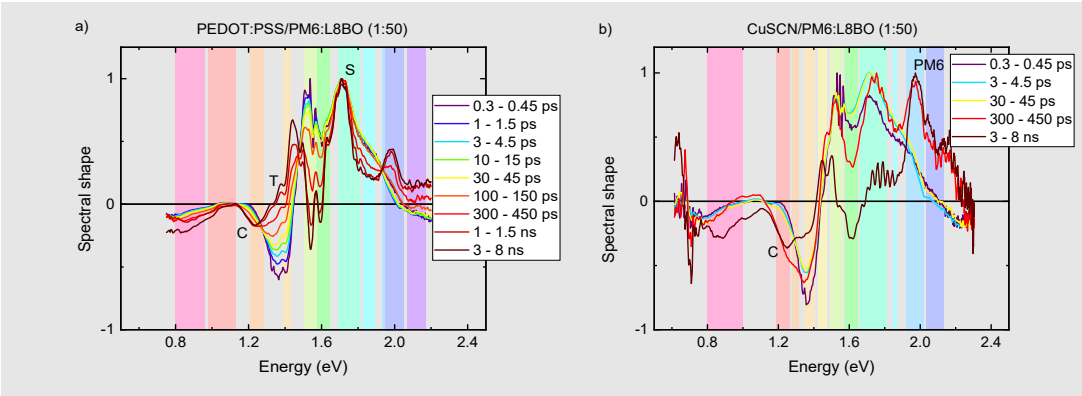

Figure S16: Charge generation in L8BO with 2% PM6: CuSCN (1.8 μJ/cm^2) versus PEDOT:PSS HTL (1.0 μJ/cm^2)

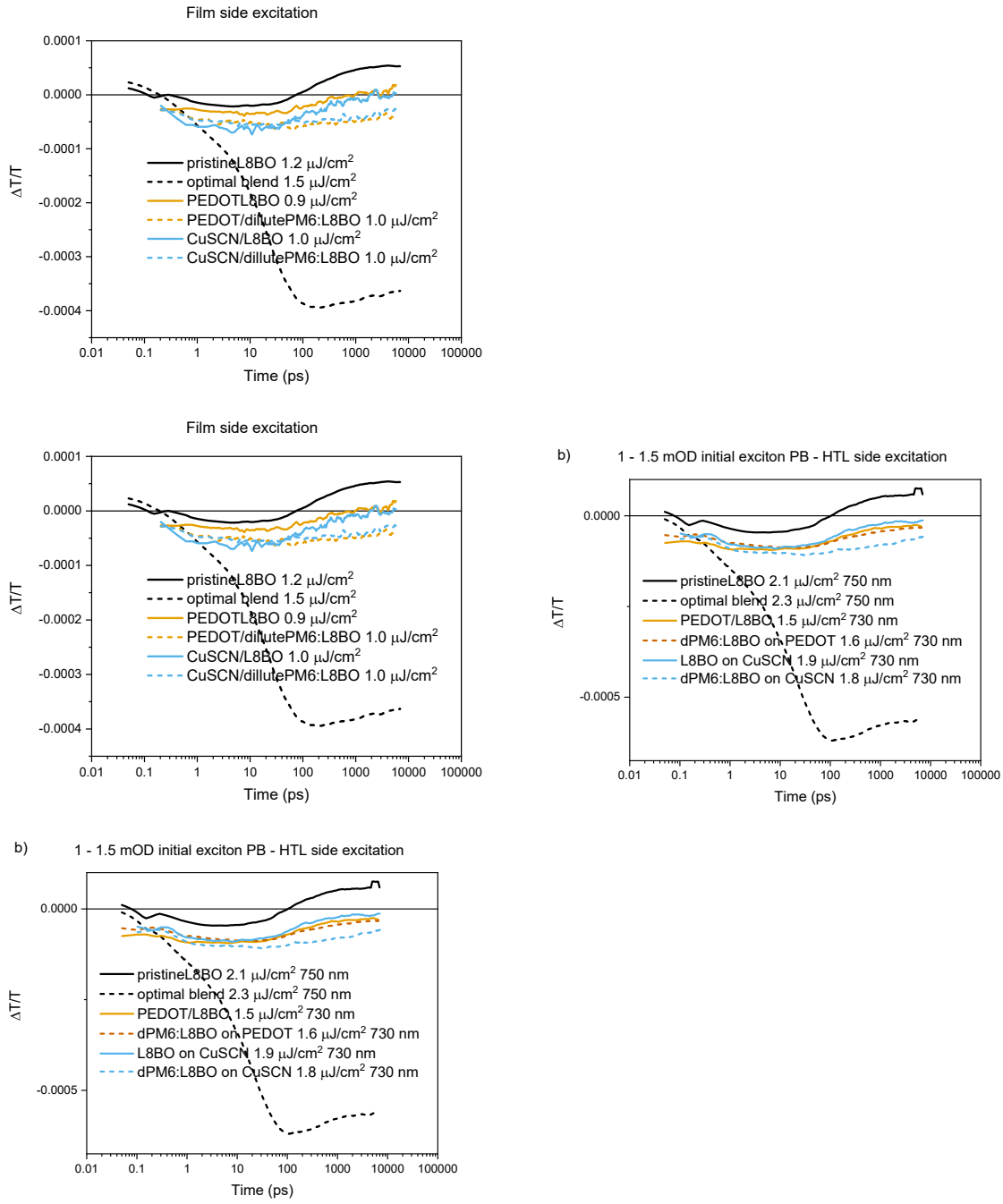

Figure S17: Influence of the excitation side on charge recombination. left: excited away from the PAL/HTL interface, right: excited close to the HTL/PAL interface.

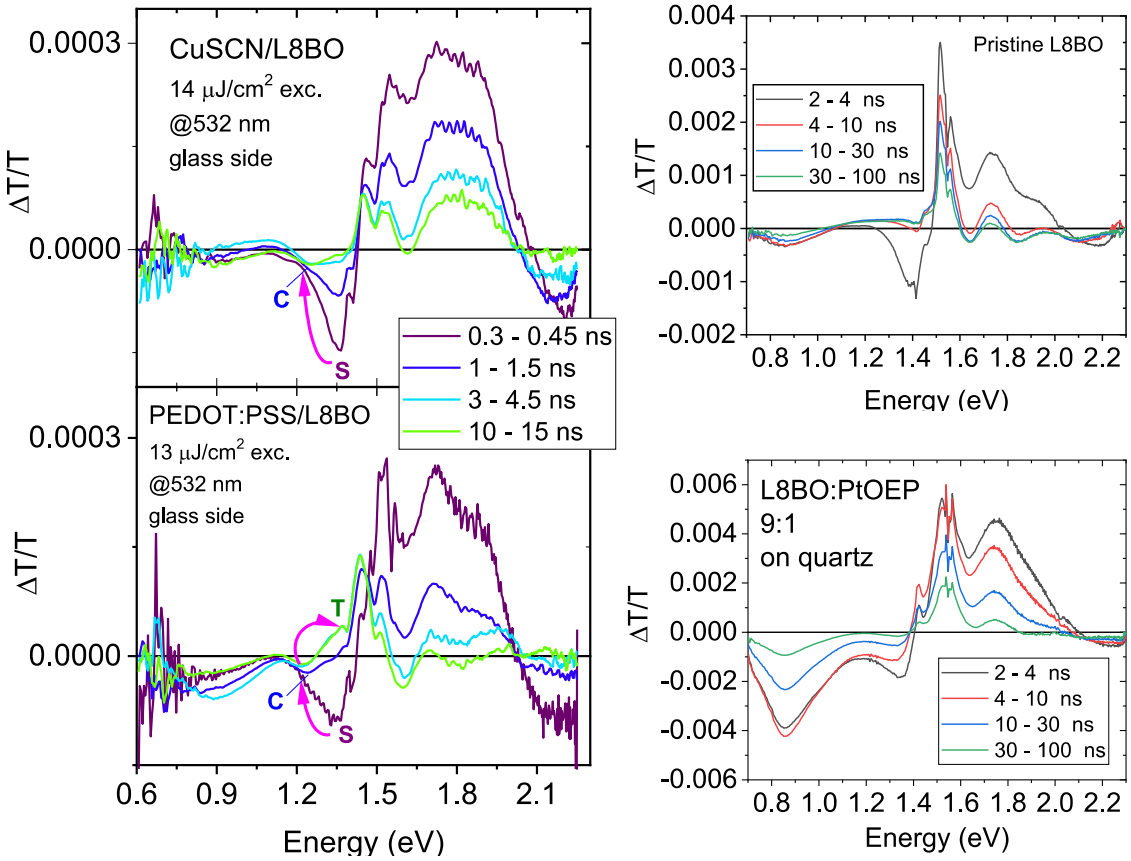

Figure S18: Spectral evidence of the formation of triplets from L8BO charges when deposited on a PEDOT:PSS HTL, contrasting with the situation with the CuSCN HTL. Note that in contrast to Figure 5c, the charge signal at 1.2 eV remains visible on the PEDOT:PSS/CuSCN films over 10 ns, nevertheless it strongly attenuated by the opposite sign contribution of the triplets. The reason is the fluence used here is lower than the one shown in Figure 4, resulting in a slower recombination/triplet formation. The spectra shown in the right panel compare pristine L8BO with L8BO containing the triplet sensitizer PtOEP. These samples were prepared by spin coating L8BO (20 mg mL^{-1} in CF with 0.5 vol.% DIO) without or with PtOEP (20 mg mL^{-1} in CF with 0.5 vol.% DIO) in vol. ratio of 9:1 (L8BO:PtOEP). The negative peak around 0.85 eV becomes more pronounced upon addition of PtOEP, confirming its association with triplet excitons. In comparison, this triplet-related peak is negligible in the CuSCN/L8BO sample for this fluence, whereas it is clearly visible in the PEDOT:PSS/L8BO sample at the same energy.

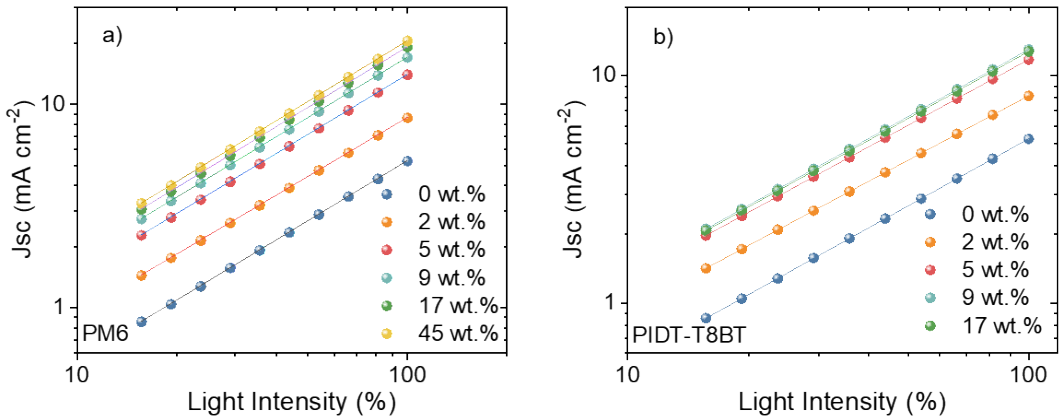

Figure S19: Jsc vs light intensity in L8BO devices with varying amounts of polymer donor a) PM6 and b) PIDT-T8BT

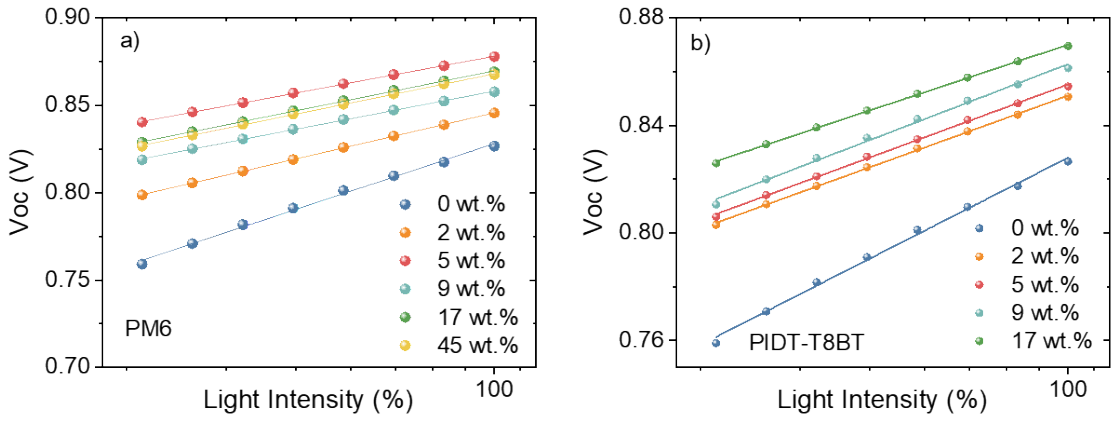

Figure S20: Voc vs light intensity in L8BO devices with varying amounts of polymer donor a) PM6 and b) PIDT-T8BT

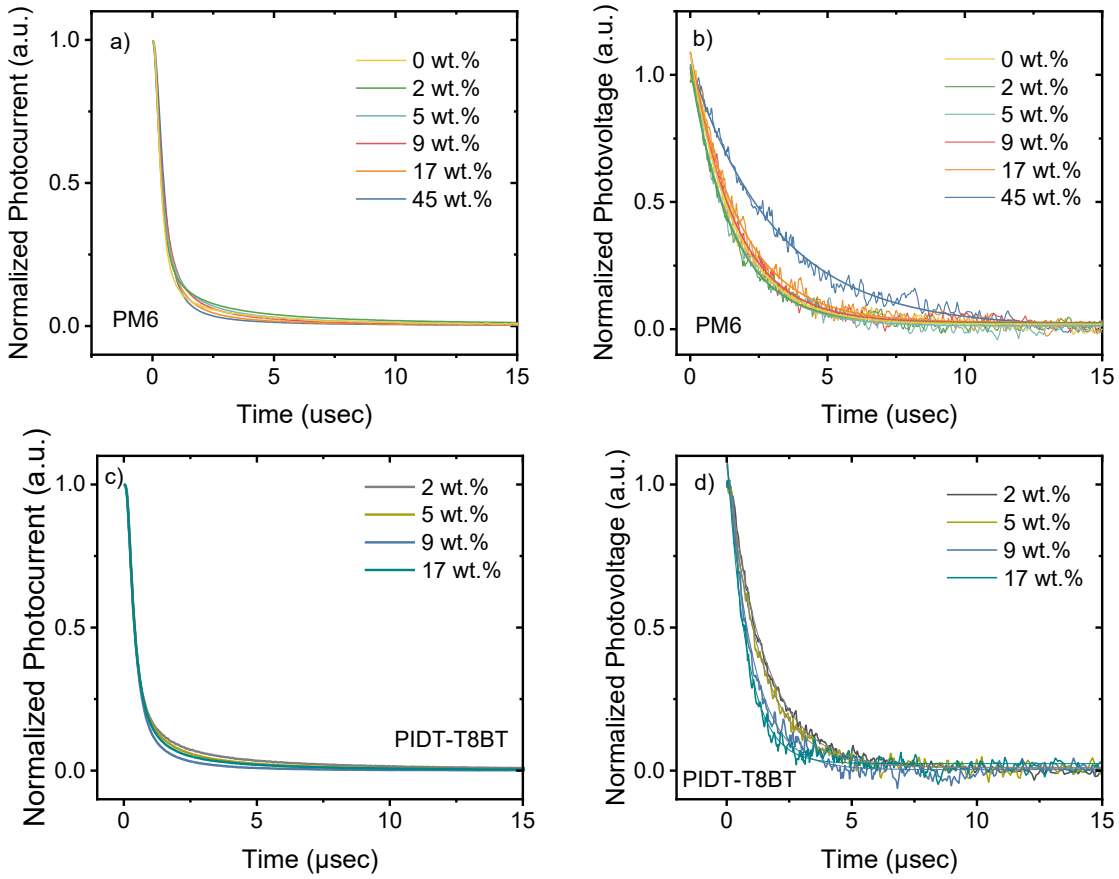

Figure S21: TPC and TPV plots showing photocurrent and photovoltage decay over time for L8BO devices with a CuSCN HTL and varying amounts of PM6 (a, b) and PIDT-T8BT (c, d).ms?

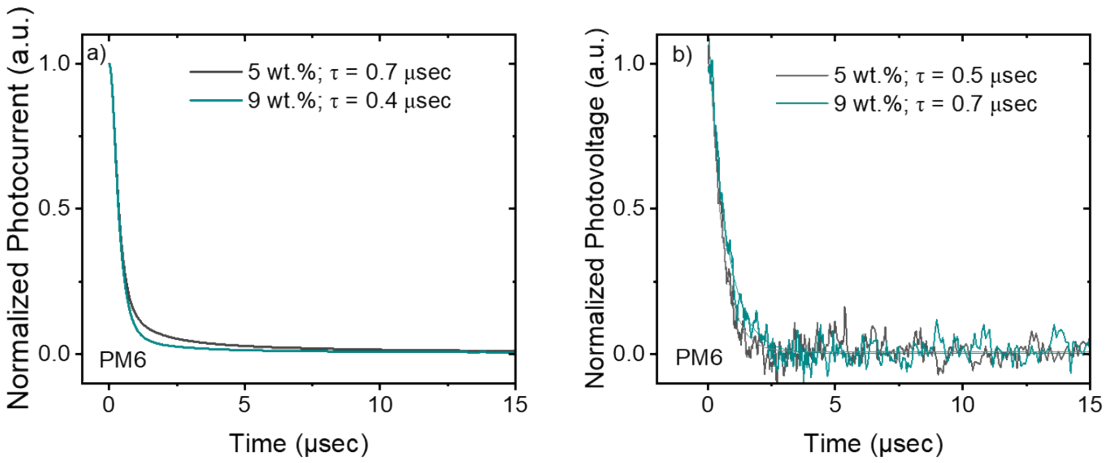

Figure S22: TPC and TPV plots showing photocurrent and photovoltage decay over time for L8BO devices with varying amounts of PM6 and a PEDOT:PSS HTL. Due to low performances when PEDOT:PSS HTL was used, TPC and TPV measurements could not be reliably performed on devices having 0 wt.% and 2 wt.% PM6.

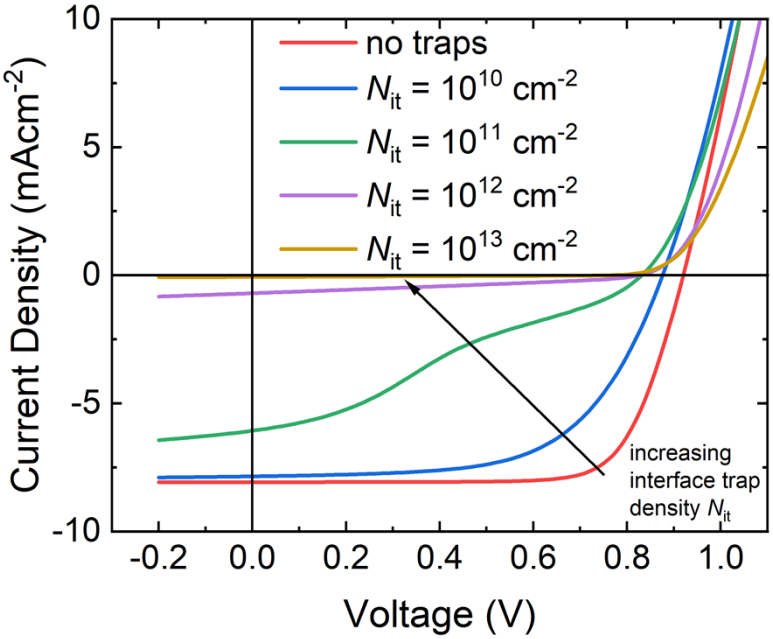

Figure S23: Simulated J-V curves of L8BO devices with varying trap density at the HTL-CuSCN interface, where for very high trap densities the J-V curves approach the case of PEDOT:PSS as the HTL.

Table S3. Summary of fitting parameters α, *n*, and the TPC and TPV lifetimes measured for L8BO devices with varying amounts of donor polymer.

Donor content (wt.%)	α	n	τ_{TPC} (µsec)	τ_{TPV} (µsec)
PM6				
0	0.98	1.80	0.82	1.6
2	0.96	1.27	0.85	1.5
5	0.98	1.01	0.80	1.6
9	0.99	1.04	0.82	1.7
17	0.99	1.10	0.73	1.8
45	0.99	1.10	0.67	3.2
PIDT-T8BT				
2	0.94	1.28	0.91	1.6
5	0.96	1.30	0.81	1.4

9	0.96	1.36	0.69	1.1
17	0.98	1.17	0.79	0.9

Reference

1. O. L. Gribkova, O. D. Iakobson, A. A. Nekrasov, V. A. Cabanova, V. A. Tverskoy and A. V. Vannikov, *J. Solid State Electrochem.*, 2016, **20**, 2991-3001.
2. M. B. Price, P. A. Hume, A. Ilina, I. Wagner, R. R. Tamming, K. E. Thorn, W. Jiao, A. Goldingay, P. J. Conaghan, G. Lakhwani, N. J. L. K. Davis, Y. Wang, P. Xue, H. Lu, K. Chen, X. Zhan and J. M. Hodgkiss, *Nature Communications*, 2022, **13**, 2827.